Dynamic Systems and Applications 32 (2023) 294-313

ANALYSIS OF VIBRATIONAL RESONANCE IN A PARAMETRIC QUINTIC OSCILLATOR WITH DOUBLE-WELL POTENTIALS

M. ANISHA NASHRIN[1], S.M. ABDUL KADER[1], M.V. SETHU MEENAKSHI[2], V. CHINNATHAMBI[1,*], S. RAJASEKAR[3]

[1]Department of Physics, Sadakathullah Appa College, Tirunelveli-627 011, Tamilnadu, India.

[2]Department of Mathematics, Fatima College, Madurai-625 018, Tamilnadu, India.

[3]School of Physics, Bharathidasan University, Tiruchirapalli 620 024, Tamilnadu, India.

*Corresponding author: veerchinnathambi@gmail.com

ABSTRACT.

The phenomenon of vibrational resonance (VR) has been investigated in a parametric quintic oscillator with five cases of double-well potential $V(x) = -\frac{1}{2}\ \omega_0^2(1 + q\cos\omega_p t)\ x^2 + \frac{1}{4}\ \beta\ x^4\ + \frac{1}{6}\gamma x^6$ while driven by both low-frequency force $f\cos\omega t$ and high-frequency force $g\cos\Omega t$ with $\Omega \gg \omega$. We restrict our analysis to the parametric choices (i) $\omega_0^2, \beta, \gamma > 0$ (double-well), (ii) $\omega_0^2, \gamma > 0$, $\beta < 0$ (double-well) (iii) $\omega_0^2, \beta > 0$, $\gamma < 0$, $4\omega_0^2\gamma < \beta^2 < \frac{16}{3}\omega_0^2\gamma$ (double-hump double-well) (iv) $\omega_0^2, \beta > 0$, $\gamma < 0$, $\beta^2 = 4\omega_0^2\gamma$ (double-hump double-well) and (v) $\omega_0^2.\beta > 0$, $\gamma < 0$, $\beta^2 > \frac{16}{3}\omega_0^2\gamma$ (double-hump double-well). For $\Omega \gg \omega$, the solution of the system consists of slow motion with frequency ω and fast motion with frequency Ω. The flow equation approach is used to drive the response amplitude $a_0(\omega)$ analytically from the equation for slow motion of the system, in terms of the parameters of the high-frequency signal and the parametric excitation. From the analytical expression of $a_0(\omega)$, we determine the values of g (denoted as g_{VR}) at which VR occurs. Numerical simulations are carried out to validate the theoretical results. We show that for fixed values of the parameters of the system, as g is varied, single or multiple vibrational resonances occur in the double-well cases of the system. g_{VR} is found to be independent of the damping strength d. Moreover, the effect of damping strength d is found to decrease the response amplitude $a_0(\omega)$.

AMS (MOS) Subject Classification. 34K18, 337C29, 65P20, 65P30, 74H65.

Key Words and Phrases. Parametric quintic oscillator, Double-well potential, Vibrational resonance, Bifurcation, Chaos.

Received August 3, 2023 ISSN 1056-2176(Print); ISSN 2693-5295 (online)

www.dynamicpublishers.org https://doi.org/10.46719/dsa2023.32.16

1. INTRODUCTION

Recently, considerable attention has been devoted both theoretically and experimentally to the phenomenon of vibrational resonance (VR), which appears in a bistable systems being excited by two periodic signals with different frequencies [1-10]. A distinctive feature of VR is that the response at the low-frequency signal passes through a maximum depending on the amplitude of an additional high-frequency modulation. Landa and McClintock [1] first reported the VR in bistable system. Later on, a theoretical treatment for analyzing VR has been proposed by Gitterman [2] and Blekhman and Landa [3]. Since this introduction, VR has now been demonstrated and analyzed theoretically, numerically and experimentally in various model systems, including communication [11,12], laser physics [13], acoustics [14], medicine [15], neuroscience [16], geosciences [17] and ecology [18]. The phenomenon has gained enormous research attention in the last two decades and has been extensively investigated due its several potential industrial and biomedical applications in a wide range of contexts including bistable systems [19,20], multistable systems [21], ratchet devices [22], excitable systems [23], quintic oscillator [24-26], coupled oscillators [27], delayed dynamical systems [26], asymmetrical potential, fractional order potential oscillators [28], neural models [29], oscillating networks [30,31], biological nonlinear systems [32], parametrically excited systems [33] and deformable potential [34], harmonically trapped and roughed potentials [35,36]. More importantly, VR has been demonstrated in experimental realizations, especially in multiple systems, arrays of hard limiters [37], bistable vertical-cavity surface emitting lasers (VCSELs) [38], and Chua circuits [39]. The potential applications of VR has been explored in, for instance, improving energy harvesting from mechanical vibrations, energy detectors [40], the detection, transmission and application of signals [41,42] and the detection of faults in bearings [43] as well as in the design of Dual Input Multiple Output (DIMO) logic gates and memory devices [44-46].

Among the various types of nonlinear systems in research on VR, parametrically driven nonlinear systems have received less attention [47-49]. Such systems are abundant in nature, however, and have a wide range of engineering applications. They are found in Bose-Einstein Condensates (BECs) models for cold atoms and laser models including semiconductor, diode and fiber lasers and VCSELs. For example, in diode lasers, high-frequency modulation is an important building block for transmitters used to encode optical communications through cavity loss or pump current modulation [50,51]. In addition parametric driving plays an important role in signal amplification, filtering and sensing, especially in macro- and nanoscale materials [52]. Recently, VR has been observed in a model Rayleigh-Plesset bubble oscillator in an incompressible fluid [53] and in a gyroscope driven by dual-frequency forcing [54]. Roy et al. [49] studied the nonlinear response of a certain parametrically driven bistable oscillator

subjected to two external periodic drives of widely different frequencies and the same authors explored the possibility of supercritical Hopf bifurcation in a typical parametric nonlinear oscillator with dual-frequency forces [55]. In this paper, we consider a parametric quintic oscillator with five cases of double-well potentials and analyze the occurrence of VR.

2. **Parametric Quintic Oscillator**

The equation of motion of the parametric quintic oscillator driven by two periodic forces is given by

$$\ddot{x} + d\dot{x} + \omega_0^2(1 + q\cos\omega_p t)x + \beta x^3 + \gamma x^5 = f\cos\omega t + g\cos\Omega t, \tag{2.1}$$

where $\Omega \gg \omega$. In Eq.(2.1), ω_0 is the natural frequency of the system without viscous damping, d is the damping coefficient, ω_p is the parametric frequency and β and γ are the cubic and quintic nonlinear coefficients. $f\cos\omega t$ is the term denoting the lower frequency drive while $g\cos\Omega t$ represents the higher frequency drive. Here (f, g) and (ω, Ω) are the amplitudes and frequencies of the low- and high-frequency drives, respectively. The parameter q is the strength of the parametric drive. The potential of the system in the absence of parametric excitation, damping and external force is

$$V(x) = \frac{1}{2}\,\omega_0^2\,x^2 + \frac{1}{4}\,\beta\,x^4\ + \frac{1}{6}\gamma x^6, \tag{2.2}$$

The potential $V(x) \to \infty$ for $\gamma > 0$ and $V(x) \to -\infty$ for $\gamma < 0$. Figure (1) depicts the shape of the potential $V(x)$ for various specific choices of the parameters ω_0^2, β and γ. The potential can be a single-well as shown in Figs. (1a) and (1c); single-well with double-hump (Figs. (1b)) and (1h); double-well (Figs.(1g)) and (1m); double-well with double-hump (Figs. (1j)), (1k) and (1l); triple-well (Figs. (1d)), (1e) and (1f) and inverted single-well (Figs. (1i)) and (1n).

The model oscillator that we are studying here is given by the following equation:

$$\ddot{x} + d\dot{x} - \omega_0^2(1 + q\cos\omega_p t)x + \beta x^3 + \gamma x^5 = f\cos\omega t + g\cos\Omega t, \quad \Omega >> \omega, \tag{2.3}$$

The minus sign before ω_0^2 in Eq.(2.3) indicates that the oscillator is a double-well potential. The function $(1 + q\cos\omega_p t)$ is always positive when the range of parameter q is $-1 < q < 1$. So the shape of the potential is always a double-well potential. The objective of the present paper is to bring in a periodic variation in the natural frequency of the oscillator with a frequency that coincides with the lower forcing frequency and the magnitude of the parametric frequency will be chosen to be $\omega_p = \omega_0$. The potential of the parametric quintic oscillator (Eq.2.3) system in the absence of damping and external forcing is

$$V(x) = -\frac{1}{2}\,\omega_0^2(1 + q\cos\omega_p t)\,x^2 + \frac{1}{4}\,\beta\,x^4\ + \frac{1}{6}\gamma x^6, \tag{2.4}$$

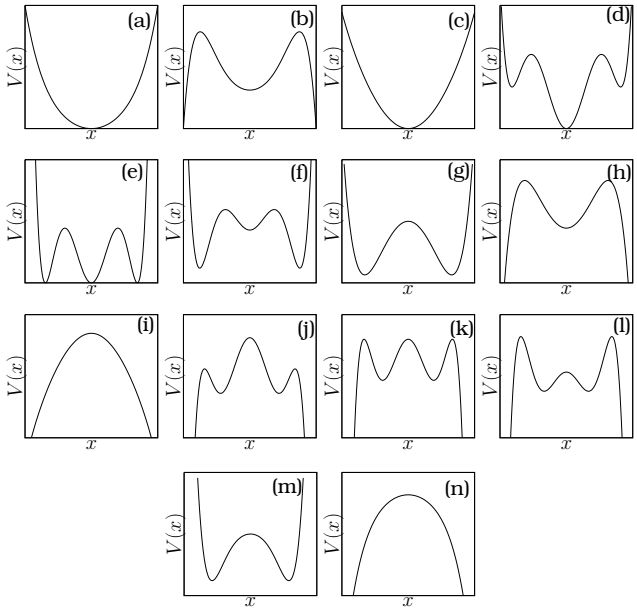

FIGURE 1. Dependence of shape of the potential of the quintic oscillator. (a) ω_0^2, β, $\gamma > 0$.(b) ω_0^2, $\beta > 0$, $\gamma < 0$. (c) ω_0^2, $\gamma > 0$, $\beta < 0$ and $\beta^2 < 4\omega_0^2\gamma$. (d) ω_0^2, $\gamma > 0$, $\beta < 0$ and $4\omega_0^2\gamma < \beta^2 < \frac{16}{3}\omega_0^2\gamma$. (e) ω_0^2, $\gamma > 0$, $\beta < 0$ and $\beta^2 = \frac{16}{3}\omega_0^2\gamma$.(f) ω_0^2, $\gamma > 0$, $\beta < 0$ and $\beta^2 > \frac{16}{3}\omega_0^2\gamma$.(g) $\omega_0^2 < 0$, β, $\gamma > 0$. (h) $\omega_0^2 > 0$, β, $\gamma < 0$. (i) ω_0^2, $\gamma < 0$, $\beta > 0$ and $\beta^2 < 4\omega_0^2\gamma$. (j) ω_0^2, $\gamma < 0$, $\beta > 0$ and $4\omega_0^2\gamma < \beta^2 < \frac{16}{3}\omega_0^2\gamma$. (k) ω_0^2, $\gamma < 0$, $\beta > 0$ and $\beta^2 = \frac{16}{3}\omega_0^2\gamma$. (l) ω_0^2, $\gamma < 0$, $\beta > 0$ and $\beta^2 > \frac{16}{3}\omega_0^2\gamma$. (m) ω_0^2, $\beta < 0$, $\gamma > 0$. (n) ω_0^2, β, $\gamma < 0$.

When $q = 0$, the potential $V(x)$ is used to model optical bistability in a dispersive medium where the refractive index is dependent on the optical intensity [56]. Equation (2.1) in the absence of external periodic forces, models a magneto-elastic beam in the nonuniform field of permanent magnets [59]. In recent years, Jeyakumari et al. studied the occurrence of VR in a quintic oscillator without parametric excitation [24,25]. In the paper, we restrict our analysis to the parametric choices in the system (Eq.2.3)

Case (i) $\omega_0^2, \beta, \gamma > 0$ (double-well) (Fig.1g),

Case (ii) $\omega_0^2, \gamma > 0$, $\beta < 0$ (double-well)(Fig.1m)

Case (iii) $\omega_0^2, \beta > 0$, $\gamma < 0$, $4\omega_0^2\gamma < \beta^2 < \frac{16}{3}\omega_0^2\gamma$(double-hump double-well)(Fig.1j)

Case (iv) $\omega_0^2, \beta > 0$, $\gamma < 0$, $\beta^2 = 4\omega_0^2\gamma$(double-hump double-well)(Fig.1k) and

Case (v) $\omega_0^2.\beta > 0$, $\gamma < 0$, $\beta^2 > \frac{16}{3}\omega_0^2\gamma$(double-hump double-well) (Fig.1l).

In the following sections, we theoretically and numerically analyze the occurrence of VR in a quintic oscillator with five cases of double-well potentials driven by both low-frequency force $f\cos\omega t$ and high-frequency force $g\cos\Omega t$ with $\Omega \gg \omega$.

3. Calculation of Response Amplitude

In this section, first we discuss how the parametric and the fast frequency drives combine to produce an effective frequency and the next section focuses on the amplitude and phase flow equations.

3.1. **The effective frequency:** Here we use the method of direct separation of motions described by Blekhman [3] as the most effective formulation of vibrational mechanics to obtain the equation of the slow motion which can be modulated by parameters of the fast driving signal analytically. For a long time $\Omega >> \omega$ and $\tau = \Omega t$, we seek the solution of Eq.(2.3) such that

$$x(t) = s(t, \omega t) + \psi(t, \Omega t). \tag{3.1}$$

If ψ is a periodic function with period $2\pi/\Omega$ or 2π-periodic function of fast time $\tau = \Omega t$ and its mean value with respect to the time τ is given by

$$< \psi(t,\tau) >= \frac{1}{2\pi}\int_0^{2\pi} \psi(t,\tau)d\tau = 0 \tag{3.2}$$

then, the aim is to obtain two systems of integral-differential equations from Eq.(2.3) such that if a pair (s, ψ) is a solution to the two integro-differential equations, then $x = s+\psi$ factoring in Eq.(3.2) completely solves Eq.(2.3). Thus substituting Eq.(3.2) in to Eq.(2.3), we have $\dot{x} = \dot{s} + \dot{\psi}$ and $\ddot{x} = \ddot{s} + \ddot{\psi}$, then

$$\begin{aligned}\ddot{s} + \ddot{\psi} + d\dot{s} + d\dot{\psi} - \omega_0^2(1 + q\cos\omega_p)s - \omega_0^2(1 + q\cos\omega_p)\psi + \beta(s^3 + 3s^2\psi + 3s\psi^2 + \psi^3) + \\ \gamma(s^5 + 5s^4\psi + 5s\psi^4 + 10s^3\psi^2 + 10s^2\psi^3 + \psi^5) = f\cos\omega t + g\cos\Omega t.\end{aligned} \tag{3.3}$$

Using Eq.(3.2) and averaging the Eq.(3.3) with respect to fast time τ, we have

$$\begin{aligned}\ddot{s} + \ddot{\psi} + d\dot{s} + d\dot{\psi} - sF_0(t) - \psi F_0(t) + \beta\left(s^3 + 3s^2\psi + 3s\psi^2 + \psi^3\right) \\ -\beta\left[(\psi^3 - < \psi^3 >) + 3s^2(\psi - < \psi >) + 3s(\psi^2 - < \psi^2 >)\right] \\ +\gamma\left[s^5 + 5s^4\psi + 5s\psi^4 + 10s^3\psi^2 + 10s^2\psi^3 + \psi^5\right] \\ -\gamma\left[(\psi^5 - < \psi^5 > +5s^4(\psi - < \psi >) + 5s(\psi^4 - < \psi^4 >)\right] \\ -\gamma\left[10s^3(\psi^2 - < \psi^2 >) + 10s^2(\psi^3 - < \psi^3 >)\right] = f\cos\omega t + g\cos\omega t.\end{aligned} \tag{3.4}$$

Because ψ is a fast motion, we assume that $\ddot{\psi} \gg \dot{\psi}, \psi, \psi^2, \psi^3, \psi^4, \psi^5$. This allows us to split the Eq.(3.4) into the following equation of motion for s and ψ.

$$\ddot{s} + d\dot{s} - sF_0(t) + \beta F_1(s,\psi) + \gamma F_2(s,\psi) = f\cos\omega t. \tag{3.5}$$

$$\ddot{\psi} + d\dot{\psi} - \psi F_0(t) + \beta F_3(s,\psi) + \gamma F_4(s,\psi) = g\cos\Omega t, \tag{3.6}$$

where

$$F_0(t) = \omega_0^2(1 + q\cos\omega_p t) \tag{3.7}$$

$$F_1(s,\psi) = s^3 + 3s^2 < \psi > +3s < \psi^2 > + < \psi^3 > \tag{3.8}$$

$$F_2(s,\psi) = s^5 + 5s^4 < \psi > +5s < \psi^4 > +10s^3 < \psi^2 > +10s^2 < \psi^3 > + < \psi^5 > \tag{3.9}$$

$$F_3(s,\psi) = (\psi^3 - < \psi >^3) + 3s^2(\psi - < \psi >) + 3s(\psi^2 - < \psi >^2) \tag{3.10}$$

$$F_4(s,\psi) = (\psi^5 - < \psi >^5) + 5s^4(\psi - < \psi >) + 5s(\psi^4 - < \psi >^4) + 10s^3(\psi^2 - < \psi >^2) \\ +10s^2(\psi^3 - < \psi >^3) \tag{3.11}$$

In Eq.(3.6), since the terms βF_3 and γF_4 are smaller than the others, we ignore it and proceed to solve the rest of the equation self-consistently (first stopping the parametrically oscillating term, solving the rest of the equation, and finally re-invoking this term) to obtain the equation

$$\ddot{\psi} + d\dot{\psi} = gB\cos(\Omega t + \phi) + gQ\left[\cos(\chi t + \alpha) + \cos(\xi t + \alpha)\right], \tag{3.12}$$

where χ, ξ are new frequencies and B, Q are new amplitude factors, which are defined as

$$\chi = \Omega + \omega_p, \qquad \xi = \Omega - \omega_p \tag{3.13a}$$

$$B = [(\Omega^2 - \omega_0^2)^2 + d^2\Omega^2]^{1/2}/\Omega(\Omega^2 + d^2)^{1/2} \tag{3.13b}$$

$$Q = \frac{qA}{2} \tag{3.13c}$$

where A is a dimensionless parameter and is given by

$$A = \frac{\omega_0^2}{\Omega\sqrt{\Omega^2 + d^2}} \tag{3.14}$$

Also, the new phase terms are

$$\alpha = \tan^{-1}\left[\frac{d}{\Omega}\right] \tag{3.15}$$

$$\phi = \tan^{-1}\left[\frac{d\Omega}{\Omega^2 - \omega_0^2}\right] \tag{3.16}$$

The solution of Eq.(3.12) evaluates with three term forcing terms and is given by

$$\psi(t) = \frac{g}{\mu_1}\cos(\Omega t + \phi + \theta) + \frac{g}{\mu_2}\cos(\chi t + \alpha + \delta) + + \frac{g}{\mu_3}\cos(\xi t + \alpha + \nu) \tag{3.17}$$

Substituting the first and second derivatives of $\psi(t)$ in Eq.(3.12) and equating the coefficients, we get the additional amplitudes and phase terms are

$$\mu_1 = \frac{\Omega^2(\Omega^2 + d^2)}{\sqrt{(\Omega^2 - \omega_0^2)^2 + \Omega^2 d^2}}, \qquad \theta = \tan^{-1}(d/\Omega) \tag{3.18}$$

$$\mu_2 = \frac{2\chi\Omega}{q\omega_0^2}\left[(\chi^2 + d^2)(\Omega^2 + d^2)\right]^{1/2}, \quad \delta = \tan^{-1}(d/\chi) \tag{3.19}$$

$$\mu_3 = \frac{2\xi\Omega}{q\omega_0^2}\left[(\xi^2 + d^2)\,(\Omega^2 + d^2)\right]^{1/2}, \quad \nu = \tan^{-1}(d/\xi) \tag{3.20}$$

Next we find the average of $< \psi^2 >, < \psi^3 >, < \psi^4 >$ and $< \psi^5 >$. Already we know that the high-frequency periodic functions constituting the form of $\psi(t)$ in Eq.(3.17) confirm the average of $\psi(t)$ over a complete period is zero. From Eq.(3.17), the average of $\psi(t)$ are $< \psi >=< \psi^3 >=< \psi^5 >= 0$, $< \psi^2(t) >= \frac{g^2}{2}\sum \frac{1}{\mu_i^2}$ and $< \psi^4(t) >= \frac{3}{8}g^4 \sum \frac{1}{\mu_i^4}$, where $i = 1, 2, 3$. The values of the averages of the $< \psi(t) >$, $< \psi^2 >, < \psi^3 >, < \psi^4 >$ and $< \psi^5 >$ can be invoked in Eq.(3.5) to obtain the following equation for the slow variable $s(t, \omega t)$ with the help of Eq.(3.5), which is

$$\ddot{s} + d\dot{s} + (\overline{\omega}^2 - \omega_0^2 q \cos\omega_p t)s + \left[(\beta + 10\gamma < \psi^2 >)s^3 + \gamma s^5\right] = f\cos\omega t \tag{3.21}$$

and the new frequency term is given by

$$\begin{aligned} \overline{\omega}^2(g) &= 3\beta' < \psi^2 > +5\gamma < \psi^4 > -\omega_0^2 \\ &= \frac{3}{2}g^2\beta' \sum_{i=1}^{3} \frac{1}{\mu_i^2} + \frac{15}{8}g^4 \sum_{i=1}^{3} \frac{1}{\mu_i^4} - \omega_0^2 \end{aligned} \tag{3.22}$$

From Eq.(3.21), we defined the time dependent effective frequency and the effective potential as

$$\omega_{eff}(t) = \sqrt{\overline{\omega}^2 - \omega_0^2 q\cos\omega_p t}, \tag{3.23}$$

$$V_{eff}(s,t) = \frac{1}{2}\omega_{eff}^2(t)s^2 + \frac{1}{4}\beta' s^4 + \frac{1}{6}\gamma s^6 \tag{3.24}$$

where

$$\begin{aligned} \beta' &= \beta + 10\gamma < \psi^2 >= \beta + 10\gamma \frac{g^2}{2} \sum_{i=1}^{3} \frac{1}{\mu_i^2} \\ &= \beta + 5\gamma g^2 \sum_{i=1}^{3} \frac{1}{\mu_i^2} \end{aligned} \tag{3.25}$$

3.2. **The flow equations:** Now we shall derive the amplitude-flow and the phase-flow equations from Eq.(3.21). Recalling the main objective of the present paper which as mentioned in the Sec.2 is to study the nonlinear response when the frequency of the parametric oscillation coincides with that of the low-frequency drive, ie. $\omega = \omega_p$. Now we rewrite the Eq.(3.21) with $\omega_p = \omega$, then

$$\ddot{s} + d\dot{s} + \left(\overline{\omega}^2(g) - \omega_0^2 q\cos\omega t\right)s + \beta' s^3 + \gamma s^5 = f\cos\omega t \tag{3.26}$$

The main objective of the present work is to study the nonlinear response when the frequency of the parametric oscillation (ω_p) coincides with the low-frequency drive (ω) called the primary resonance, that is, by tuning ω close to the frequency $\overline{\omega}$ given by Eq.(3.22). To do this, we introduce a detuning parameter $\overline{\sigma}$, such that $\omega = \overline{\omega} + \epsilon\overline{\sigma}$, where ϵ is a perturbation parameter. To apply the perturbation technique, Eq.(3.26) is rearranged as follows

$$\ddot{s} + \overline{\omega}^2 s = \epsilon\left[-d\dot{s} + \omega_0^2 q(\cos\omega t)s - \beta' s^3 - \gamma s^5 + f\cos\omega t\right] \tag{3.27}$$

Introducing the dimensionless time $\tau = \omega t$ and rescaled the parameters $\frac{\overline{\omega}^2}{\omega^2} = 1 - \epsilon\sigma, \Gamma = \frac{d}{\omega^2}, \Lambda = \frac{\beta'}{\omega^2}, \alpha = \frac{\gamma}{\omega^2}, f = F\omega^2$ and $K = \frac{\omega_0}{\omega^2}$, then we can rearrange the Eq.(3.27) as

$$\ddot{s} + s = \epsilon\left[-\Gamma\dot{s} + K\cos\tau s + \Lambda s^3 + \alpha s^5 + f\cos\tau + \sigma s\right] \tag{3.28}$$

The flow equations can be arrived at through the method of averaging, the details of which have described in refs.[60,61]. For using the method of averaging we can write $s = u\cos\omega t - v\sin\omega t$ with $u(t) = a(t)\cos\theta(t)$ and $v(t) = a(t)\sin\theta(t)$ and proceeding as usual [60,61], we arrive at the amplitude and phase flow equations

$$\dot{a} = -\omega\left[\Gamma a + F\sin\theta\right], \tag{3.29}$$

where $F = \frac{f}{\omega^2}$ and $\Gamma = d/\omega^2$

$$\dot{\theta} = \omega\left[-\sigma + \frac{3}{4}\Lambda a^2 + \frac{5}{8}\alpha a^4 - \frac{F}{a}\cos\theta\right] \tag{3.30}$$

For the fixed points (a_0, θ_0) of this dynamical system, we obtain the following expression in the modified detuning parameter σ as,

$$\sigma = \left[\frac{3}{4}\Lambda a_0^2 + \frac{5}{8}\alpha a_0^4\right] \pm \sqrt{\frac{F^2}{a_0^2} - \Gamma^2} \tag{3.31}$$

Now substitute the value of σ (Eq.(3.31)) in the modified detuning parameter, then $\overline{\omega}^2 = \omega^2 - \epsilon\omega^2\sigma$, ie., $\frac{\overline{\omega}^2}{\omega^2} = 1 - \epsilon\sigma$,

$$\overline{\omega}^2 = \omega^2 - \epsilon\left\{\left[\frac{3\beta' a_0^2}{4} + \frac{5}{8}\gamma a_0^4\right] \pm \sqrt{\frac{f^2}{a_0^2} - d^2\omega^2}\right\} \tag{3.32}$$

Substituting the value of β' in Eq.(3.22), we get

$$\overline{\omega}^2 = \frac{3}{2}g^2\beta\sum_{i=1}^{3}\frac{1}{\mu_i^2} + \frac{75}{8}\gamma g^4\sum_{i=1}^{3}\frac{1}{\mu_i^4} - \omega_0^2 \tag{3.33}$$

Now combining the Eqs.(3.32) and (3.33), we get

$$\frac{3}{2}g^2\beta\sum_{i=1}^{3}\frac{1}{\mu_i^2} + \frac{75}{8}\gamma g^4\sum_{i=1}^{3}\frac{1}{\mu_i^4} - \omega_0^2 = \omega^2 - \epsilon\left\{\left[\frac{3\beta' a_0^2}{4} + \frac{5}{8}\gamma a_0^4\right] \pm \sqrt{\frac{f^2}{a_0^2} - d^2\omega^2}\right\} \tag{3.34}$$

or

$$\frac{3}{2}g^2\beta'\sum_{i=1}^{3}\frac{1}{\mu_i^2} + \frac{15}{8}\gamma g^4\sum_{i=1}^{3}\frac{1}{\mu_i^4} - \omega_0^2 = \omega^2 - \epsilon\left\{\left[\frac{3\beta' a_0^2}{4} + \frac{5}{8}\gamma a_0^4\right] \pm \sqrt{\frac{f^2}{a_0^2} - d^2\omega^2}\right\} \tag{3.35}$$

(3.36)

$$\frac{3}{2}g^2\beta'\sum_{i=1}^{3}\frac{1}{\mu_i^2} + \frac{15}{8}\gamma g^4\sum_{i=1}^{3}\frac{1}{\mu_i^4} = (\omega^2 + \omega_0^2) - \epsilon\left\{\left[\frac{3\beta' a_0^2}{4} + \frac{5}{8}\gamma a_0^4\right] \pm \sqrt{\frac{f^2}{a_0^2} - d^2\omega^2}\right\}$$

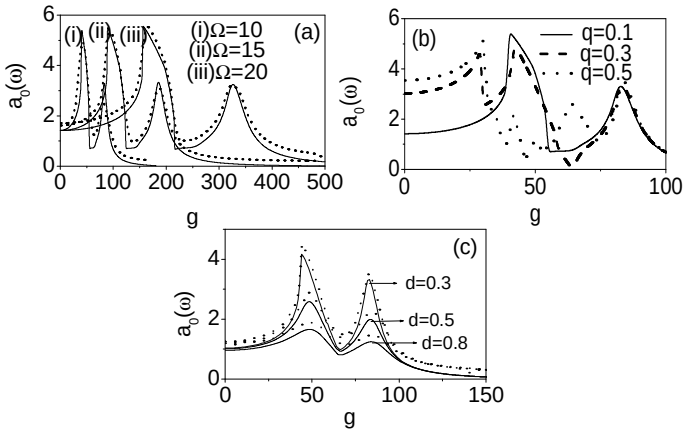

FIGURE 2. (a) Theoretically and numerically calculated $a_0(\omega)$ represented by continuous curve and painted circles respectively for a few values of Ω with $q = 0.1$ and $d = 0.3$ (b) Theoretical response amplitude $a_0(\omega)$ for a few values of q with $\Omega = 10$ and $d = 0.3$ and (c) Theoretically and numerically calculated $a_0(\omega)$ represented by continuous curve and painted circles respectively for a few values of d with $\Omega = 10$ and $q = 0.1$. The simulation parameters are $\omega = \omega_p = \omega_0 = 1.0, \beta = 1.0, \gamma = 1.0$ and $f = 0.05$.

In the following sections, we consider the system (2.3) with five double-well cases of the potential $V(x)$ separately and analyze the vibrational resonance (VR) using Eq.(3.36) and verify the theoretical results numerically.

4. **Analysis of VR**

In this section, we investigate the effects of the different parameters (q, d and Ω) of the system (Eq.2.3) with five cases of double-well potentials on the response amplitude $a_0(\omega)$. To compare with the theoretical $a_0(\omega)$ given by Eq. (3.36), we compute $a_0(\omega)$ from the numerical solution of Eq. (2.3). Numerical $a_0(\omega)$ is given by

$$a_0(\omega) = \frac{\sqrt{a_0(\omega)_{\rm s}^2 + a_0(\omega)_{\rm c}^2}}{f}, \tag{4.1a}$$

where

$$a_0(\omega)_{\rm s} = \frac{2}{nT}\int_0^{nT} x(t)\sin\omega t{\rm d}t, \quad a_0(\omega)_{\rm c} = \frac{2}{nT}\int_0^{nT} x(t)\cos\omega t{\rm d}t \tag{4.1b}$$

with $T = 2\pi/\omega$ and $n = 200$.

4.1. **VR with Double-well potential, ($\omega_0^2, \beta, \gamma > 0$):** For $\omega_0^2, \beta, \gamma > 0$, $V(x)$ is a double-well potential. We fix the parameters as $\beta = \gamma = 1, f = 0.05$ and $\omega = \omega_p = \omega_0 = 1$. Figure 2(a) shows g versus $a_0(\omega)$ for three values of $\Omega = 10, 15$ and 20 respectively. Continuous curves represent theoretical result obtained from Eq.(3.36).

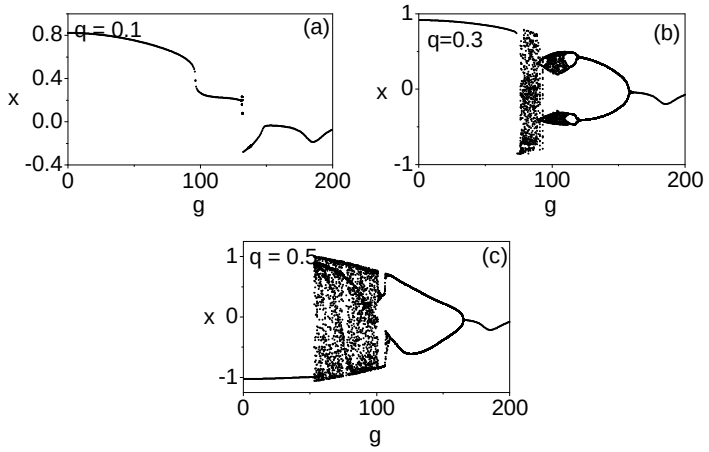

FIGURE 3. Bifurcation diagrams of equation (2.3) with $\Omega = 15, d = 0.3$ for three values q. The values of x are collected at $t = n \times 2\pi/\omega, \quad n = 1, 2, ..., 200$. The values of the other parameters are $\omega = \omega_p = \omega_0 = 1.0, \beta = 1.0, \gamma = 1.0$ and $f = 0.05$.

Painted circles represent numerically calculated $a_0(\omega)$ from Eq.(4.1). Numerically computed $a_0(\omega)$ is in well agreement with the theoretical approximation. In Fig.2(a), for all values of Ω, two resonances occur with nearly equal peak values. The first and second resonances occur at $g = (40.98, 83.07)$ for $\Omega = 10$, $g = (92.29, 187.13)$ for $\Omega = 15$ and $g = (160.03, 325.15)$ for $\Omega = 20$. For $\Omega = 10$ and $\Omega = 15$, the motion is unbounded when $g > 178$ and $g > 445$. From Fig.2a, we clearly observed that as the value of Ω increases, the position of the peaks increases in the direction of g and the width of the first and second resonances also increases. The analytical frequency-response curves obtained for three values of $q = 0.1, 0.3, 0.5$ respectively and presented in Fig.2(b). For $q = 0.1$, two resonances occur at $g = (40.98, 83.03)$, three resonances occur at $g = (20.70, 42.42, 83.07)$ for $q = 0.3$ and five resonances occur at $g = (29.64, 42.34, 50.47, 63.68, 83.07)$ for $q = 0.5$. We clearly see that the number of resonances increases as the amplitude of the parametric excitation q increases, and the effect of q on $a_0(\omega)$ is a shift in the peak position in the opposite direction of g. Figure 2(c) illustrates the effect of damping d on resonance. The maximum of the resonance (g_{VR}) is unchanged by the damping strength (d). However, the response amplitude $a_0(\omega)$ at the resonance decreases with increase in d.

Since the system (Eq.2.3) can exhibit variety of bifurcations of periodic orbit leading to chaotic motion and bifurcations of chaotic attractor, we examined the occurrence of them using bifurcation diagram and phase portrait. For certain cases of the parametric choices considered in our study, chaotic motion is found for sufficiently large values of the control parameter g, particularly far after resonance. For this purpose, we numerically solve this equation (2.3) using the fourth order Runge-Kutta algorithm with fixed step sizes $\Delta t = 0.001$. The values of the following parameters were

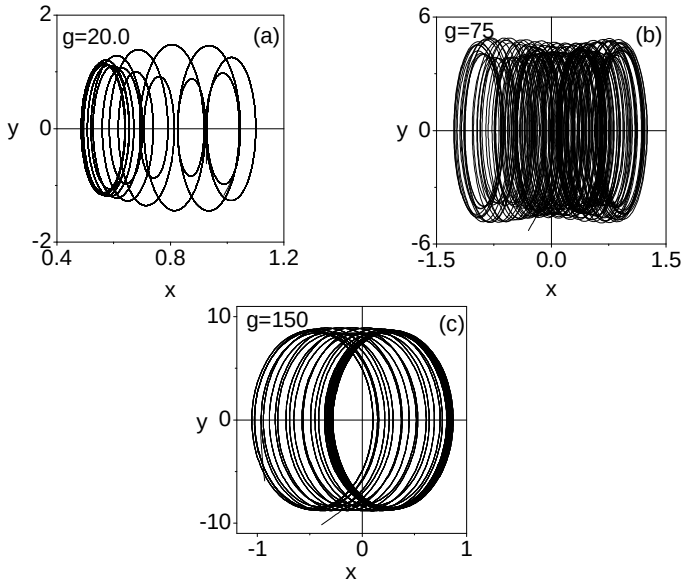

FIGURE 4. Phase portraits of actual motion of the system (Eq.2.3) showing the (a) period-1 orbit, (b) chaotic attractors and (c) period-2 orbit with the parameters of Fig.3(c).

fixed as follows: $d = 0.3, \beta = \gamma = 1.0, \Omega = 15, f = 0.05$ and $\omega = \omega_p = \omega_0 = 1.0$. The initial conditions are $x(0) = 1$ and $\dot{x}(0) = 1.0$ and the time is $t = 4000$ with the first 100 iterates dropped as transients. Figure 3 shows the bifurcation diagram of Eq.(2.3) for three values of $q = 0.1, 0.3$ and 0.5. We restricted our analysis to the range $0 < g < 200$. For $q = 0.1$, the period-T is found (Fig.3a) in the above range of g. When $q = 0.3$, chaotic motion, antimonotonicity and reverse periodic orbits are found for $g \in [74.629, 122.225]$. This is shown in Fig.3(b). In Fig.3(c), corresponding to the above parametric choices with $q = 0.5$, chaotic motion and other periodic orbits are found. As q increases, the spacing of the chaotic region increases which is clearly seen in Figs.3(b) and 3(c). An example of periodic and chaotic attractor is shown in Figs.4(a-c).

4.2. **VR with Double-well potential, ($\omega_0^2, \gamma > 0, \beta < 0$):** In this section we consider the system (Eq.2.3) with the double-well potential of the form shown in Fig.1(m), where $\omega_0^2 > 0, \gamma > 0$ and $\beta < 0$. First we consider the effect of frequency Ω of the high-frequency excitation on VR. We fix the parameters as $\beta = -1, \gamma = 1, f = 0.05$ and $\omega = \omega_p = \omega_0 = 1.0$. Figure 5(a) shows the plot of $a_0(\omega)$ for three values of $\Omega = (10, 15, 20)$ with $q = 0.1$ and $d = 0.3$ computed from Eq.(3.36) and superimposed with their corresponding numerical curves computed from Eq.(4.1) for comparison. One can obviously see that the theoretical and numerical results are in close agreement. Double resonances occur for all the values of Ω. For instance, first and second resonances occur for $\Omega = 10, 15, 20$ at $g = (101.068, 124.471), (220.999, 274.343)$ and $(375.952, 472.481)$ with nearly equal peaks of first and second resonances. However

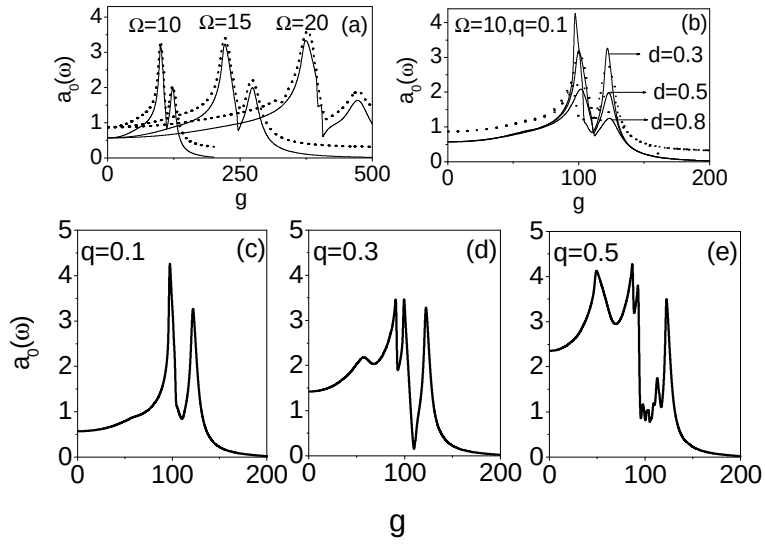

FIGURE 5. Theoretically and numerically calculated $a_0(\omega)$ represented by continuous curve and painted circles respectively for a few values of (a) Ω with $q = 0.1$ and $d = 0.3$ (b) d with $\Omega = 10$ and $q = 0.1$. (c-e) Theoretically calculated $a_0(\omega)$ for a few values of q with $\Omega = 10$ and $d = 0.3$. The simulation parameters are $\omega = \omega_p = \omega_0 = 1.0, \beta = -1.0, \gamma = 1.0$ and $f = 0.05$.

the position of the peaks is shifted further away from the origin as the value of Ω increases. To examine the effect of damping d on the system's response, we show the dependence of the response amplitude $a_0(\omega)$ on the amplitude g of the high-frequency signal for three values of damping parameter $d = (0.3, 0.5, 0.8)$ in Fig.5(b) for $\Omega = 10, q = 0.1$ and other parameters are stated as in Fig.5(a). The continuous lines represent theoretical values while the painted lines represent the corresponding numerical values of $a_0(\omega)$. The effect of the damping parameter d on the response curve is obvious. In Fig.5(b), we notice close agreement between theoretical $a_0(\omega)$ and numerically computed $a_0(\omega)$. The maximum value of $a_0(\omega)$ is reduced by increasing the value of d. Then we analyze analytically the effect of q on VR. Figures 5(c-e) shows the plot of $a_0(\omega)$ for three values of $q = (0.1, 0.3, 0.5)$ with $\Omega = 10, d = 0.3$ and other parameters are unchanged. From this figure, we clearly observe that the number of resonances increases as the value of q increases. For example, two resonances occur for $q = 0.1$ whereas four and seven resonances occur for $q = 0.3$ and $q = 0.5$.

4.3. **VR with Double-hump Double-well potential- ($\omega_0^2, \beta > 0, \gamma < 0, 4\omega_0^2\gamma < \beta^2 < \frac{16}{3}\omega_0^2\gamma$):** $V(x)$ is a double-hump double-well potential (Fig.1j) for $\omega_0^2, \beta > 0, \gamma < 0$, $4\omega_0^2\gamma < \beta^2 < \frac{16}{3}\omega_0^2\gamma$. For this type of potential, we investigate the effects of different parameters Ω, q and d on the response amplitude $a_0(\omega)$. First we analyze the effect of Ω on $a_0(\omega)$. We fix the values of the parameters in the system (Eq.2.3) as $\beta = 1, \gamma = -1, f = 0.05, d = 0.3, q = 0.3$ and $\omega = \omega_p = \omega_0 = 1.0$. Analytical

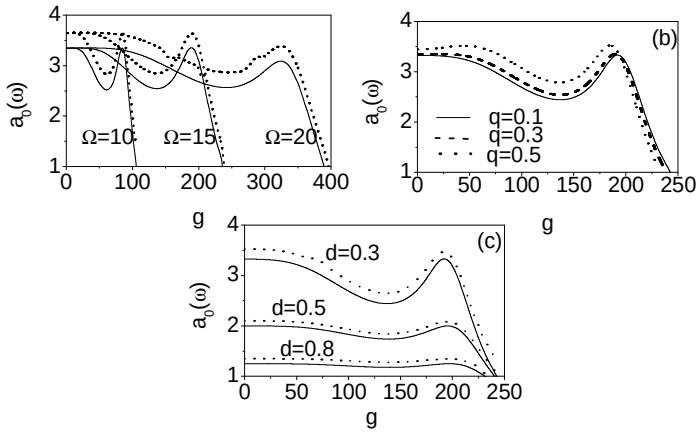

FIGURE 6. (a) Theoretically and numerically calculated $a_0(\omega)$ represented by continuous curve and painted circles respectively for a few values of Ω with $q = 0.3$ and $d = 0.3$ (b) Theoretical response amplitude $a_0(\omega)$ for a few values of q with $\Omega = 15$ and $d = 0.3$ and (c) Theoretically and numerically calculated $a_0(\omega)$ represented by continuous curve and painted circles respectively for a few values of d with $\Omega = 15$ and $q = 0.3$. The simulation parameters are $\omega = \omega_p = \omega_0 = 1.0, \beta = 1.0, \gamma = -1.0$ and $f = 0.05$.

and numerical response curves for three values of $\omega = 10, 15$ and 20 are presented in Fig.6(a). Single resonance is observed for all the values of Ω. It also appears that the resonance width expands with increasing the values of Ω. For $\Omega = 10, 15$ and 20, resonances occur at $g = 85.021, 188.651$ and 322.772 respectively. The motion is unbounded when $g > 106.01$ for $\Omega = 10$, $g > 237.07$ for $\Omega = 15$ and $g > 389.18$ for $\Omega = 20$ which is clearly seen in Fig.6(a). Next we consider the effect of q on VR. Figure 6(b) shows the theoretical response amplitude $a_0(\omega)$ as a function of g for a few values of $q = (0.1, 0.3, 0.5)$. In Fig.6(b), we notice that a single resonance with nearly equal response amplitude $a_0(\omega)$ is observed for all values of q. Figure 6(c) illustrates the effect of damping parameter d on resonance. Maximum of the resonance g_{VR} is unchanged by the damping strength. However $a_0(\omega)$ at the resonance decreases with increase in d which is clearly seen in Fig.6(c).

The actual motions of the system (Eq.2.3) with double-hump double-well potential (Fig.1j) is studied through the bifurcation diagram for the parametric choices considered in Fig.6. Figure 7 shows the bifurcation diagrams of the system (Eq.2.3) with double-hump double-well potential. We restricted our analysis to the range $0 < g < 200$. From Fig.7, period-T solution is found in the range $g \in [0, 115.99]$ for $q = 0.1$ (Fig.7(a)), $g \in [0, 76.26]$ for $q = 0.3$ (Fig.7(b)) and $g \in [0, 67.84]$ for $q = 0.5$ (Fig.7(c))). Chaotic motion and other periodic orbits are observed when $g > 115.99$ for $q = 0.1$, $g > 76.26$ for $q = 0.3$ and $g > 67.84$ for $q = 0.5$ respectively. From Fig.7, we see that the range of periodic orbits decreases as q increases.

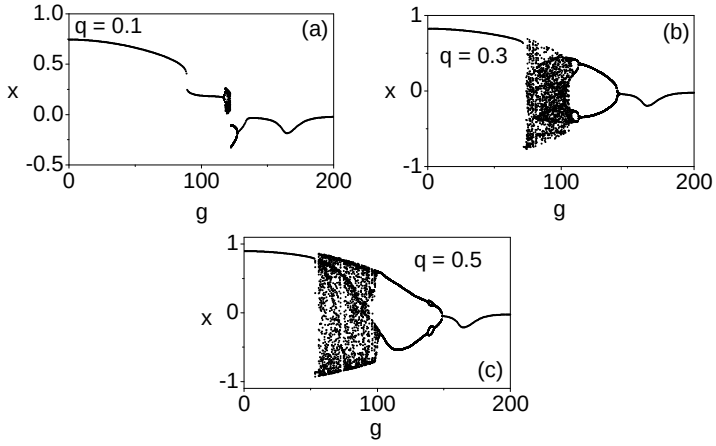

FIGURE 7. Bifurcation diagrams showing period-doubling phenomenon, chaotic dynamics and reverse period-doubling phenomenon for a few values of $q = (0.1, 0.3, 0.5)$. The values of x are collected at $t = n \times 2\pi/\omega, \quad n = 1, 2, ..., 200$. The values of the parameters are $\omega = \omega_p = \omega_0 = 1.0, \beta = 1.0, \gamma = -1.0, \Omega = 15, d = 0.3$ and $f = 0.05$.

4.4. **VR with Double-hump Double-well potential- ($\omega_0^2, \beta > 0, \gamma < 0$, $\beta^2 = \frac{16}{3}\omega_0^2\gamma$):** In this section, we consider the system (Eq.2.3) with the double-hump double-well potential of the form in Fig.1(k) where $\omega_0^2, \beta > 0, \gamma < 0$, $\beta^2 = \frac{16}{3}\omega_0^2\gamma$. We begin our examination of the resonance phenomenon in the system by first considering the effect of Ω. We fix the parameters values of the system as $\beta = 1.0, \gamma = -1.9, q = 0.3, d = 0.3$ and $\omega = \omega_p = \omega_0 = 1.0$. As expected for this case, VR is observed as shown in Fig.8(a). In fact, the results of the analysis for the system with $\Omega = 10, 15$ and 20 in Fig.8(a) are consistent with both theoretical and numerical results. The continuous lines are the response curves of theoretically computed $a_0(\omega)$ values while the painted lines represent corresponding numerical values. For $\Omega = 10$ and 15, single resonance occurs at $g = 201.101$ and $g = 448.772$. For $\Omega = 20$, $a_0(\omega)$ decreases continuously when g increases, that is, no resonance occurs. The motion is unbounded when $g > 214.860$ for $\Omega = 10$ and when $g > 479.047$ for $\Omega = 15$. Figure 8(b) shows the theoretical response amplitude $a_0(\omega)$ as a function of g for a few values of q. When $g < 160.671$, the value of $a_0(\omega)$ decreases continuously as g increases, and no resonance is observed. A single resonance is observed for all values of q with equal peaks when $g > 160.671$, which is clearly seen in Fig.8(b). Figure 8(c) illustrates the effect of damping on resonance is unchanged by the damping strength. However, $a_0(\omega)$ at the resonance decreases with increase in d.

4.5. **VR with Double-hump Double-well potential, ($\omega_0^2, \beta > 0, \gamma < 0$, $\beta^2 > \frac{16}{3}\omega_0^2\gamma$):** Finally, we consider the system (Eq.2.3) with the double-hump double-well potential of the form in Fig.1(l) where $\omega_0^2, \beta > 0, \gamma < 0$, $\beta^2 > \frac{16}{3}\omega_0^2\gamma$. We fix $\beta = 1.5, \gamma = -0.19, f = 0.05$ and $\omega = \omega_p = \omega_0 = 1.0$. For this potential form, we now

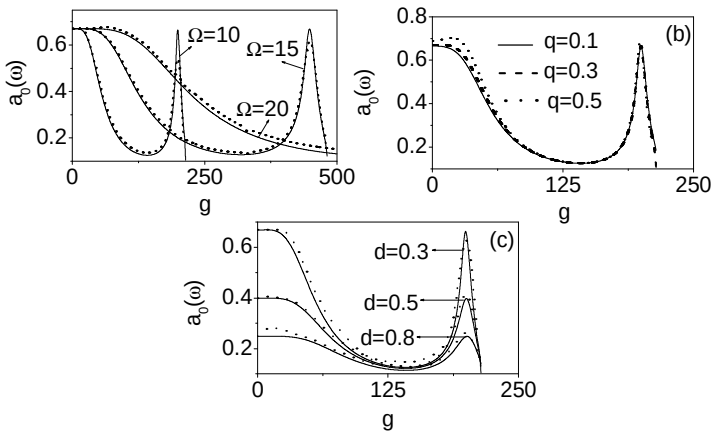

FIGURE 8. (a)Theoretically and numerically calculated $a_0(\omega)$ represented by continuous curve and painted circles respectively for a few values of Ω with $q = 0.3$ and $d = 0.3$ (b) Theoretical response amplitude $a_0(\omega)$ for a few values of q with $\Omega = 10$ and $d = 0.3$ and (c) Theoretically and numerically calculated $a_0(\omega)$ represented by continuous curve and painted circles respectively for a few values of d with $\Omega = 10$ and $q = 0.3$. The simulation parameters are $\omega = \omega_p = \omega_0 = 0.3, \beta = 1.0, \gamma = -1.9$ and $f = 0.05$.

proceed to verify the existence of VR in the presence of biharmonic signal by varying the parameters Ω, q and d. Figure 9(a) shows the dependence of response amplitude $a_0(\omega)$ on g for three values of $\Omega = 10, 15, 20$ with $d = 0.3$ and $q = 0.5$. Theoretically and numerically calculated $a_0(\omega)$ represented by continuous curve and painted circles respectively. Numerically computed $a_0(\omega)$ is in well agreement with the theoretical approximation. For $\Omega = 10$, the response amplitude $a_0(\omega)$ is found to be maximum at $g = 253.651$. For $\Omega = 15$ and 20 as g increases, $a_0(\omega)$ decreases and resonance is not observed which is clearly seen in Fig.9(a). The influence of q and d is shown in Figs.9(b) and 9(c). In Fig.9(b), we have plotted the analytical results of $a_0(\omega)$ against g for three values of $q = 0.1, 0.3$ and 0.5. Single resonance is observed for all values of q and g_{VR} is unchanged when q increases from small value. In Fig.9(b), no resonance occurs in the interval $0 < g < 227.13$. Figure 9(c) shows the plot of $a_0(\omega)$ versus g for three values of $d = 0.3, 0.5$ and 0.8. The effect of damping on resonance is unchanged by the damping strength. However, the response amplitude $a_0(\omega)$ decreases with increase in d.

5. **Conclusion**

We have analyzed the phenomenon of vibrational resonance (VR) in a parametrically driven quintic oscillator with five cases of double-well potentials. Besides the

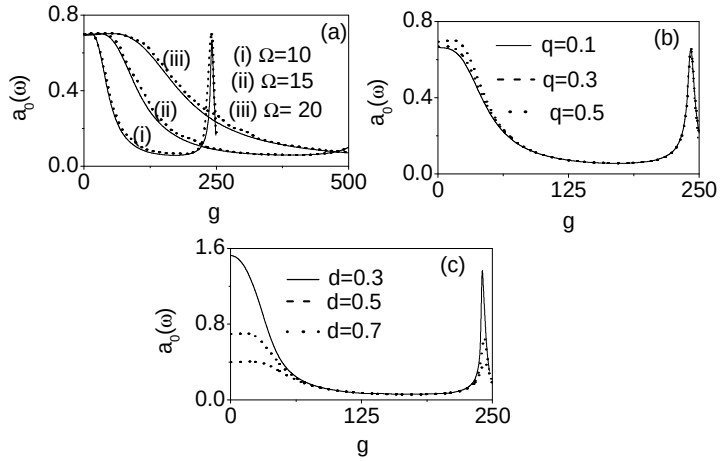

FIGURE 9. (a)Theoretically and numerically calculated $a_0(\omega)$ represented by continuous curve and painted circles respectively for a few values of Ω with $q = 0.5$ and $d = 0.3$ (b) Theoretical response amplitude $a_0(\omega)$ for a few values of q with $\Omega = 10$ and $d = 0.3$ and (c) Theoretical response amplitude $a_0(\omega)$ for a few values of d with $\Omega = 10$ and $q = 0.5$. The simulation parameters are $\omega = \omega_p = \omega_0 = 1.0, \beta = 1.5, \gamma = -0.19$ and $f = 0.05$.

parametric excitation, the oscillator is subjected to two other drives, one with a low-frequency (ω) that is equal to the frequency of the parametric drive (ω_p) and the other of a much higher frequency (Ω). Our main focus here is to analyze VR through the periodic variation of in the natural frequency (ω_0) of the oscillator with a frequency corresponding to the lower frequency (ω). Using the flow equation approach, we have derived a functional relation between the nonlinear response amplitude ($a_0(\omega)$) and the strength of the high-frequency drive (g). From the analytical expression of ($a_0(\omega)$), we determined the number of resonances and the values of the control parameters, say, g or q or Ω at which resonance occurs. In the five cases of double-well potential, when g is varied we found either no resonance or multiple resonances depending on the values of the other parameters of the system. As g is varied we obtain the following results. (i) Double or multiple resonances occur for a range of values of parameters q, d and Ω in double-well cases of the system. (ii) In the system with double-hump double-well potential cases, no resonance or a single resonance occurs for a range of values of the parameters of the system q, d and Ω. By examining the bifurcation diagram in Poincaré section and the phase space structures, the underlying dynamics associated with the phenomenon of VR is elucidated. We conclude that, for the system with double-well potential cases, there are two distinct dynamical mechanisms that can provide resonances, depending on the parameters of the system: (i) a monotonic increase in the size of a chaotic attractor and (ii) bifurcation from a periodic attractor to a chaotic attractor of larger period.

REFERENCES

[1] P.S. Landa and P.V.E. McClintock, Vibrational resonance, *J. Phys.A: Math. Gen.*, 33: L433-L438, 2000.

[2] M. Gittermann, Bistable oscillator driven by two periodic fields, *J. Phys. A: Math. Gen.*, 34: L355-L357, 2001.

[3] I.I. Blechman and P.S. Landa, Conjugate resonances and bifurcations in nonlinear systems under biharmonical excitation, *Int. J. Non-Linear Mech.*, 39: 421-426, 2004.

[4] A.A. Zaikin, L. Lopez, J.P. Baltanas, J. Kurths and M.A.F. Sanjuan, Vibrational resonance in a noise-induced structure, *Phys.Rev.E*, 66: 011106-4, 2002.

[5] E. Ullner, A. Zaikin, J. Garcia-Ojalvo, R. Bascones and J. Kurths, Vibrational resonance and vibrational propagation in excitable systems, *Physics Letters A*, 312: 348-354, 2003.

[6] J.P. Baltanas, L. Lopez, I.I. Blechman, P.S. Landa, A. Zaikin, J. Kurths and M.A.F. Sanjuan, Experimental evidence, numerics,and theory of vibrational resonance in bistable systems, *Phys. Rev. E*, 67: 066119-7, 2003.

[7] V.N. Chizhevsky, E. Smeu and G. Giacomelli, Experimental evidence of vibrational resonance in an optical system, *Phys. Rev. Lett.*, 91: 220602-4, 2003.

[8] J. Casado-Pascual and J.P. Baltanas, Effects of additive noise on vibrational resonance in a bistable system, *Phys. Rev. E*, 69: 046108, 2004.

[9] V.N. Chizhevsky and G. Giacomelli, Experimental and theoretical study of the noise-induced gain degradation in vibrational resonance, *Phys. Rev. E*, 66: 011106, 2004.

[10] V.N. Chizhevsky and G. Giacomelli, Improvement of signal-to-noise ratio in a bistable optical system: Comparison between vibrational and stochastic resonance, *Phys. Rev. A*, 71: 011801(R), 2005.

[11] H.C. Gerhardt, Significance of two frequency bands in long distance vocal communications in the green tree frog, *Nature*, 261: 692-694, 1976.

[12] G.P. Agrawal, *Fiber-Optic Communication Systems*, Wiley, New York, 1992.

[13] D.C. Su, M.H. Chiu and C.D. Chen, Simple two-frequency laser, *Precis. Eng.*, 18(2-3): 161-163, 1996.

[14] A.O. Maksimov, On the subharmonic emission of gas bubbles under two-frequency excitation, *Ultrasonics*, 35: 79-86, 1997.

[15] K. Harikrishnan and G. Ambika, Resonance phenomena in discrete systems with bichromatic input signal, *Eur. Phys. J. B*, 61(3): 343-353, 2008.

[16] D.M. Ackermann, N. Bhadra, E.L. Foldes and K.L. Kilgore, Conduction block of whole nerve without onset firing using combined high frequency and direct current, *Med. Biol. Eng. Comput.*, 49(2): 241-251, 2011.

[17] L. Ridolfi, P.D. Odorico and F. Laio, Vegetation dynamics induced by phreatophyte- water table interactions, *J. Theor. Biol.*, 248(2): 301-310, 2007.

[18] C. Jeevarathinam, S. Rajasekar and M.A.F. Sanjuan, Vibrational resonance in groundwater-dependent plant ecosystems, *Ecol. Complex*, 15: 33-42, 2013.

[19] S. Rajasekar and M.A.F. Sanjuan, *Nonlinear Resonances*, Springer, Switzerland, 2016.

[20] J. Baltanas, L. Lopez, I.I. Blechman, P.S. Landa, A. Zaikin, J. Kurths and M.A.F. Sanjuan, Experimental evidence, numerics, and theory of vibrational resonance in bistable systems, *Phys. Rev. E*, 67(6): 066119, 2003.

[21] T. Roy-Layinde, J. Laoye, O. Popoola, U.E. Vincent and P.V.E. McClintock, Vibrational resonance in an inhomogeneous medium with periodic dissipation, *Phys. Rev. E*, 96(3): 032209, 2017.

[22] L. Du, W. Song, W. Guo and D. Mei, Multiple current reversals and giant vibrational resonance in a high-frequency modulated periodic device, *Eur. Phys. Lett.*, 115(4): 4000-8, 2016.

[23] B. Deng, J. Wang, X. Wei, H. Yu and H. Li, Theoretical analysis of vibrational resonance in a neuron model near a bifurcation point, *Phys. Rev. E*, 89(6): 062916, 2014.

[24] S. Jeyakumari, V. Chinnathambi, S. Rajasekar and M.A.F. Sanjuan, Single and multiple vibrational resonance in a quintic oscillator with monostable potentials, *Phys. Rev.E*, 80: 046608, 2009.

[25] S. Jeyakumari, V. Chinnathambi, S. Rajasekar and M.A.F. Sanjuan, Analysis of vibrational resonance in a quintic oscillator, *Chaos*, 19: 043128-8, 2009.

[26] W. Guo and L. Ning, Vibrational resonance in a fractional order quintic oscillator system with time delay feedback, *Int. J. Bifur. Chaos*, 30(02): 2050025, 2020.

[27] P. Sarkar and D.S. Ray, Vibrational antiresonance in nonlinear coupled systems, *Phys. Rev. E*, 99(5): 052221, 2019.

[28] J. Yang, D. Huang, M.A.F. Sanjuan and H. Liu, Vibrational resonance in an overdamped system with a fractional order potential nonlinearity, *Int. J. Bifur. Chaos*, 28(07): 1850082, 2018.

[29] M. Ge, L. Lu, Y. Xu, R. Mamatimin, Q. Pei and Y. Jia, Vibrational mono-/bi-resonance and wave propagation in fitzhugh-nagumo neural systems under electromagnetic induction, *Chaos Soliton & Fractal*, 133: 109645, 2020.

[30] Y. Qin, C. Han, Y. Che and J. Zhao, Vibrational resonance in a randomly connected neural network, *Cogn Neurodyn*, 12(5): 509-518, 2018.

[31] V. Baysal and E. Yilmaz, Effects of electromagnetic induction on vibrational resonance in single neurons and neuronal networks, *Phys. A: Stat. Mech. Appl.*, 537: 122733, 2020.

[32] L. Ning and Z. Chen, Vibrational resonance analysis in a gene transcriptional regulatory system with two different forms of time-delays, *Physica D: Nonlinear Phenomena*, 401: 132164, 2020.

[33] P. Sarkar, S. Paul and D.S. Ray, Controlling subharmonic generation by vibrational and stochastic resonance in a bistable system, *J. Stat. Mech.: Theory Exp.*, 2019(6): 063211, 2019.

[34] U.E. Vincent, T. Roy-Layinde, O. Popoola, P. Adesina and P.V.E. McClintock, Vibrational resonance in an oscillator with an asymmetrical deformable potential, *Phys. Rev. E*, 98(6): 062203, 2018.

[35] J. Laoye, T. Roy-Layinde, K. Omoteso, O. Popoola and U.E. Vincent, Vibrational resonance in a higher-order nonlinear damped oscillator with rough potential, *Pramana-J. Phys.*, 93(6): 1-10, 2019.

[36] K. Abirami, S. Rajasekar and M.A.F. Sanjuan, Vibrational resonance in a harmonically trapped potential system. Commun., *Commun. Nonlinear Sci. Numer. Simul.*, 47: 370-378, 2017.

[37] Y. Ren and F. Duan, Theoretical and experimental implementation of vibrational resonance in an array of hard limiters, *Phys. A: Stat. Mech. Appl.*, 456: 319-326, 2016.

[38] V. Chizhevsky, Amplification of optical signals in a bistable verticalcavity surface-emitting laser by vibrational resonance, *Philos. Trans. R. Soc. A*, 379(2192): 20200241, 2021.

[39] B. Usama, S. Morfu and P. Marquie, Vibrational resonance and ghost vibrational resonance occurrence in chua's circuit models with specific nonlinearities, *Chaos, Solitons & Fractals*, 153: 111515, 2021.

[40] Y. Ren, Y. Pan and F. Duan, Generalized energy detector for weak random signals via vibrational resonance, *Phys. Lett. A*, 382(12): 806-810, 2018.

[41] C. Yao, Z. He, T. Nakano and Y. Qian, Inhibitory-autapse enhanced signal transmission in neural networks, *J. Shuai, Nonlinear Dyn.*, 97(2): 1425-1437, 2019.

[42] P. Jia, J. Yang and Y. Leng, The echo chirp signal amplification by the vibrational information fusion method, *Int. J. Mod. Phys. B*, 34(06): 2050041, 2020.

[43] L. Xiao, X. Zhang, S. Lu, T. Xia and L. Xi, A novel weak-fault detection technique for rolling element bearing based on vibrational resonance, *J. Sound Vib.*, 438: 490-505, 2019.

[44] P.R. Venkatesh and A. Venkatesan, Vibrational resonance and implementation of dynamic logic gate in a piecewise-linear murali-lakshmanan-chua circuit, *Commun. Nonlinear Sci. Numer. Simul.*, 39: 271-282, 2016.

[45] P.R. Venkatesh, A Venkatesan and M. Lakshmanan, Implementation of dynamic dual input multiple output logic gate via resonance in globally coupled duffing oscillators, *Chaos*, 27(8): 083106, 2017.

[46] Y. Yao and J. Ma, Logical stochastic and vibrational resonances induced by periodic force in the fitzhugh-nagumo neuron, *Eur. Phys. J. Plus*, 137(11): 1214, 2022.

[47] J. Yang, M.A.F. Sanjuan and H. Liu, Bifurcation and resonance in a fractional Mathieu Duffing oscillator, *Eur. Phys. J, B*, 88: 310, 2015.

[48] S. Ghosh and D. Shankar Ray, Optical Bloch equations in a biharmonic field: Vibrational resonance, *Eur. Phys. J, B*, 88: 1434-1436, 2015.

[49] S. Roy, D. Das and D. Banerjee, Nonlinear response of a parametric bistable oscillator with multiple excitations, *Eur. Phys. J, B*, 93: 1-7, 2015.

[50] C. Mayol, R. Toral, C.R. Mirasso, S.I. Turovets and L. Pesquera, Theory of main resonance in directly modulated diode lasers, *IEEE J. Quantum Electron*, 38(3): 260-269, 2002.

[51] S. Bennet and C.M. Snowden Iezekiel, Nonlinear dynamics in directly modulated multiple quantum-well lasers diode, *IEEE J. Quantum Electron*, 33(11): 2076-2083, 1997.

[52] A.A. Seshia, M. Palaniapan, T.A. Roessig, R.T. Howe, R.W. Gooch, T.R. Schimert and S. Montague, A vacuum packaged surface micromechanical resonant accelerometer, *J. Microelectromech. Syst.*, 11(6): 784-793, 2002.

[53] K.A. Omoteso, T.O. Roy-Layinde, J.A. Laoye, U.E. Vincent and P.V.E. McClintock, Acoustic vibrational resonance in a Rayleigh-Plesset bubble oscillator, *Ultrasonics - Sonochemistry*, 70: 105346, 2021.

[54] K.S. Oyeleke, O.I. Olusola, U.E. Vincentc, D. Ghosh and P.V.E. McClintock, Parametric vibrational resonance in a gyroscope driven by dual-frequency forces, *Physics Letters A*, 387: 127040, 2021.

[55] S. Roy, D. Das and D. Banerjee, Hopf Bifurcation in vibrational resonance through modulation of fast frequency, *arXiv:2205.08091v1 [nlin.CD]*, 17 May 2022.

[56] Y.H. Kao and C.S. Wang, Analog study of bifurcation structures in a Van der Pol oscillator with a nonlinear restoring force, *Phys. Rev. E*, 48: 2514, 1993.

[57] G. Gilboa, N. Sochen and Y.Y. Zeevi, Image Sharpening by Flows Based on Triple Well Potentials, *J. Math. Imag. & Vision*, 20: 121-131, 2004.

[58] C. Wagner and T. Kiefhaber, Intermediates can accelerate protein folding, *Proc.Natl. Acad. Sci. USA*, 96(12): 6716-6721, 1999.

[59] G.Z. Li and F.C. Moon, Criteria for chaos of a three-well potential oscillator with homoclinic and heteroclinic orbits, *J. Sound Vibr.*, 136: 17-34, 1990.

[60] A.H. Nayfeh, *Perturbation Methods*, John Wiley & Sons, 2008. ISBN: 3527617612, 9783527617616

[61] K. Al-Zubi, *Response of an oscillator with a Duffing parameter of the fifth power*, B.Sc., Degree thesis, Delft University of Technology, Netherlands, 2019. An electronic version of this thesis is available at http://repository.tudelft.nl/.